

# Finite-size scaling of coherence and steered coherence in the Lipkin-Meshkov-Glick model

Ming-Liang Hu,<sup>1,2,\*</sup> Fan Fang,<sup>3</sup> and Heng Fan<sup>2,4,5,†</sup>

<sup>1</sup>*School of Science, Xi'an University of Posts and Telecommunications, Xi'an 710121, China*

<sup>2</sup>*Institute of Physics, Chinese Academy of Sciences, Beijing 100190, China*

<sup>3</sup>*School of Electronic Engineering, Xi'an University of Posts and Telecommunications, Xi'an 710121, China*

<sup>4</sup>*CAS Center for Excellence in Topological Quantum Computation, University of Chinese Academy of Sciences, Beijing 100190, China*

<sup>5</sup>*Songshan Lake Materials Laboratory, Dongguan 523808, China*

Quantum coherence reflects the origin of quantumness and might be capable of extracting the subtle nature of a system. We investigate the ground-state coherence and steered coherence in the Lipkin-Meshkov-Glick model and show that they detect faithfully the quantum phase transitions of this model. Moreover, we carry out scaling analysis on the coherence and steered coherence by using the continuous unitary transformation method, and it is found that they show different scaling behaviors in different phase regions of this model. These results may provide useful insights into the mechanism underlying quantum criticality in many-body systems.

PACS numbers: 03.65.Yz, 64.70.Tg, 75.10.Pq;

## I. INTRODUCTION

Quantum phase transition (QPT) is a purely quantum phenomenon which originates from quantum fluctuations [1]. Besides the traditional method, it has also been widely studied by virtue of concepts borrowed from quantum information theory in the past two decades. This is mainly carried out based on singular behaviors of the variety of quantum correlations. For example, the ground-state entanglement of two carefully chosen sublattices or neighboring spins detect successfully QPTs of certain spin systems [2–6]. Moreover, the quantum discord of two very short distance spins can also detect QPTs in some one-dimensional spin systems [7–9].

As the origin of quantumness and a fundamental property of quantum states not available in classical physics, quantum coherence remains one of the research focuses of quantum theory since the beginning of the 20th century, and it may underlie singularity of quantum critical behaviors of various condensed matter systems. In particular, since the formulation of the resource theory of coherence [9–11], the investigation of QPTs from the aspect of the ground-state coherence has been given more attention due to its fundamentality. In fact, its feasibility has been validated through studying those one-dimensional spin models, including the spin-1/2 Ising and  $XX$  models [12], the  $XY$  [13–16] and the general  $XYZ$  models [17], as well as the spin-1  $XXZ$  model [18].

Starting from the coherence measures, one can not only interpret those already known quantum correlations [19–23] but also introduce other quantifiers of quantumness [24–28]. One of these coherence-based quantifiers is the steered coherence for a bipartite state  $\rho_{AB}$ , including the average steered coherence (ASC) with respect to the mutually unbiased bases [24–26] and the maximal steered coherence (MSC) in the eigenbasis of  $\rho_B = \text{tr}_A \rho_{AB}$  [28]. The feasibility of the ASC in signaling QPTs has been validated for certain spin systems [29, 30], and

compared with entanglement and quantum discord, it has the benefit of being long ranged, thus releases the strict restriction on the choice of special spins for probing QPTs.

While the above works are mainly on the one-dimensional systems, the coherence in high-dimensional systems might exhibit more rich phenomenon due to the high coordinate number. One of these models is the Lipkin-Meshkov-Glick (LMG) model. It was first introduced in nuclear physics [31–33] and recent studies showed that it can be simulated in trapped ions [34, 35], nitrogen-vacancy center ensembles [36], and superconducting qubits [37]. It has also found applications in quantum information processing [38, 39]. For these reasons, we investigate coherence and steered coherence in the LMG model with emphasis on their capability in characterizing the quantum criticality. We will consider the following three cases: (i) the thermodynamic limit case by using the semiclassical approach, (ii) the isotropic case which is exactly solvable with arbitrary system size  $N$ , and (iii) the anisotropic case by utilizing the continuous unitary transformation (CUT) technique [40, 41]. The results show that both the coherence and steered coherence detect QPT of the LMG model faithfully, and their dependence on the system size  $N$  is found to be scaled with different exponents in different phase regions. These observations show a robust pathway to explore quantum criticality in many-body systems using the coherence and coherence-based quantities.

The structure of this paper is as follows. In Sec. II, we recall some preliminaries on quantifying coherence and steered coherence, then in Sec. III, we present their solutions for the LMG model. Sec. IV is devoted to analyzing their behaviors and their scaling exponents in different phase regions. Finally, we summarize the main results in Sec. V.

## II. PRELIMINARIES

In this section, we recall briefly two measures of coherence defined within the resource theoretic framework and the related characterization of steered coherence. For a state described by the density operator  $\rho$ , we consider its  $l_1$  norm of

\*Electronic address: mingliang0301@163.com

†Electronic address: hfan@iphy.ac.cn

coherence and relative entropy of coherence given by [10]

$$C_{l_i}^{(|i\rangle)}(\rho) = \sum_{i \neq j} |\rho_{ij}|, \quad C_{re}^{(|i\rangle)}(\rho) = S(\rho_{\text{diag}}) - S(\rho), \quad (1)$$

where  $\rho_{ij}$  denote the elements of  $\rho$  in the reference basis  $\{|i\rangle\}$ ,  $\rho_{\text{diag}}$  is a state obtained from  $\rho$  by replacing all its off-diagonal elements with zero,  $S(\rho) = -\text{tr}(\rho \log_2 \rho)$  is the von Neumann entropy of  $\rho$ , and likewise for  $S(\rho_{\text{diag}})$ .

Starting from the above coherence measures, one can then consider the steered coherence for a two-qubit state  $\rho_{AB}$ , with qubit  $A$  ( $B$ ) holding by Alice (Bob). There are two frameworks for such a problem. Within the first framework, it was formulated by considering the three mutually unbiased observables  $\{\sigma_{x,y,z}\}$  (i.e., the Pauli operators). To be explicit, Alice measures  $\sigma_i$  on qubit  $A$  and then informs Bob of her choice  $\sigma_i$  and outcomes  $a$ , based on which Bob calculates the average coherence of the collapsed states of  $B$  with respect to the eigenbases of the two  $\sigma_j \neq \sigma_i$ . After Alice finishing her measurements of  $\{\sigma_{x,y,z}\}$  with equal probability, the ASC of Bob's states can be obtained as [24]

$$C_{\alpha}^{\text{asc}}(\rho_{AB}) = \frac{1}{2} \sum_{i \neq j, a} p_{\Pi_i^a} C_{\alpha}^{\sigma_j}(\rho_{B|\Pi_i^a}), \quad (2)$$

where  $p_{\Pi_i^a} = \text{tr}(\Pi_i^a \rho_{AB})$  denotes the probability of Alice's outcome  $a$  when she measures  $\sigma_i$ ,  $\rho_{B|\Pi_i^a} = \text{tr}_A(\Pi_i^a \rho_{AB}) / p_{\Pi_i^a}$  is the collapsed state of  $B$ ,  $\Pi_i^{\pm} = (\mathbb{1} \pm \sigma_i) / 2$  is the measurement operator ( $\mathbb{1}$  is the  $2 \times 2$  identity operator), and  $\alpha = l_i$  or  $re$ . When  $C_{\alpha}^{\text{asc}}(\rho_{AB})$  is larger than a threshold, it is said that there is non-local advantage of quantum coherence which could be viewed as a quantum correlation stronger than entanglement [24].

The second framework refers to the steered coherence on  $B$  with respect to the eigenbasis  $\mathcal{B} = \{|\xi_i\rangle\}$  of  $\rho_B = \text{tr}_A \rho_{AB}$ . To be explicit, Alice first performs the positive-operator valued measurements (POVM)  $M$  on her qubit  $A$ , Bob then calculates the coherence of  $\rho_{B|M} = \text{tr}_A(M \rho_{AB}) / p_M$  in the basis  $\mathcal{B}$ , where  $p_M = \text{tr}(M \rho_{AB})$ . The MSC of qubit  $B$  can be written as [28]

$$C_{\alpha}^{\text{msc}}(\rho_{AB}) = \inf_{\mathcal{B}} \left\{ \max_{M \in \text{POVM}} C_{\alpha}^{\mathcal{B}}(\rho_{B|M}) \right\} \quad (3)$$

where the infimum over  $\mathcal{B}$  is necessary only when  $\rho_B$  is degenerate.  $C_{\alpha}^{\text{msc}}(\rho_{AB})$  is also intimately related to quantum correlations, e.g., it is maximal for any pure entangled state with full Schmidt rank and vanishes for quantum-classical states [28].

### III. SOLUTION OF COHERENCE AND STEERED COHERENCE FOR THE LMG MODEL

Spin system is a natural playground for revealing quantum characteristics and is also a candidate for building blocks implementing quantum computation and information processing tasks. The LMG model describes a system consists of  $N$  spin-1/2 particles that are mutually interacted with each other. The Hamiltonian (in units of  $\hbar$ ) reads [40, 41]

$$\begin{aligned} \hat{H} &= -\frac{\lambda}{N} \sum_{i < j} (\sigma_x^i \sigma_x^j + \gamma \sigma_y^i \sigma_y^j) - h \sum_i \sigma_z^i \\ &= -\frac{2\lambda}{N} (S_x^2 + \gamma S_y^2) - 2h S_z + \frac{\lambda}{2} (1 + \gamma), \end{aligned} \quad (4)$$

where  $\sigma_{\alpha}^i$  ( $\alpha = x, y, z$ ) represent the Pauli operators at site  $i$ ,  $\lambda$  characterizes the spin interaction (with  $\gamma$  being its anisotropy in the  $xy$  plane), and the prefactor  $1/N$  is introduced for eliminating infinity of the free energy per spin in the thermodynamic limit. Moreover,  $h$  is the transverse magnetic field and  $S_{\alpha} = \sum_i \sigma_{\alpha}^i / 2$ . In the following, we concentrate on the ferromagnetic case and we set  $\lambda = 1$  (i.e.,  $h$  will be in units of  $\lambda$ ),  $0 \leq \gamma \leq 1$ , and  $h \geq 0$  (the spectrum of  $\hat{H}$  is invariant under the substitution  $h \rightarrow -h$ ).

For such a model, its ground state lies in the maximum spin sector  $S = N/2$  [40, 41]. In the basis  $\{|\uparrow\uparrow\rangle, |\uparrow\downarrow\rangle, |\downarrow\uparrow\rangle, |\downarrow\downarrow\rangle\}$ , the two-spin reduced density matrix can be obtained as [42]

$$\rho_{ij} = \begin{pmatrix} v_1 & 0 & 0 & u \\ 0 & y & y & 0 \\ 0 & y & y & 0 \\ u & 0 & 0 & v_2 \end{pmatrix}, \quad (5)$$

and its elements are given by

$$\begin{aligned} v_{1,2} &= \frac{N^2 - 2N + 4\langle S_z^2 \rangle \pm 4(N-1)\langle S_z \rangle}{4N(N-1)}, \\ y &= \frac{N^2 - 4\langle S_z^2 \rangle}{4N(N-1)}, \quad u = \frac{\langle S_x^2 \rangle - \langle S_y^2 \rangle}{N(N-1)}, \end{aligned} \quad (6)$$

where  $v_1$  takes the “+” sign and  $v_2$  takes the “-” sign (likewise for subsequent similar notations). The expectation values  $\langle S_z \rangle$  and  $\langle S_{\alpha}^2 \rangle$  ( $\alpha = x, y, z$ ) could be obtained by virtue of different methods for the Hamiltonian (4) with different system parameters, and for  $0 \leq \gamma \leq 1$ , one also has  $u \geq 0$  [40].

From Eq. (5), one can obtain directly that there is no single-spin coherence as  $\rho_i = \text{tr}_j \rho_{ij}$  is diagonal. For  $\rho_{ij}$ , the two-spin coherence can be obtained as

$$\begin{aligned} C_{l_i}(\rho_{ij}) &= 2(y + u), \\ C_{re}(\rho_{ij}) &= 2y + \sum_{i=1}^2 (\epsilon_i \log_2 \epsilon_i - v_i \log_2 v_i), \end{aligned} \quad (7)$$

while the ASC and MSC can be obtained as (see Appendix A)

$$\begin{aligned} C_{l_i}^{\text{asc}}(\rho_{ij}) &= \sum_{i=1}^2 \left( \frac{1}{2} x_i + |y - v_i| \right) + |y + u| + |y - u|, \\ C_{re}^{\text{asc}}(\rho_{ij}) &= 2 + H_2(y + v_1) \\ &\quad - \sum_{i=1}^2 \left[ H_2\left(\frac{1 + x_i}{2}\right) + (y + v_i) H_2\left(\frac{y}{y + v_i}\right) \right], \\ C_{l_i}^{\text{msc}}(\rho_{ij}) &= \frac{2(y + u)}{\sqrt{1 - (v_1 - v_2)^2}}, \\ C_{re}^{\text{msc}}(\rho_{ij}) &= H_2(r_{11}) - H_2\left(\frac{1 + \sqrt{(1 - 2r_{11})^2 + 4|r_{12}|^2}}{2}\right), \end{aligned} \quad (8)$$

where  $H_2(\cdot)$  is the binary Shannon entropy function, and

$$\begin{aligned} \epsilon_{1,2} &= \frac{1}{2} (v_1 + v_2 \pm \sqrt{4u^2 + (v_1 - v_2)^2}), \\ x_{1,2} &= \sqrt{4(y \pm u)^2 + (v_1 - v_2)^2}, \quad r_{12} = \frac{y + u}{\sqrt{1 - (v_1 - v_2)^2}}, \\ r_{11} &= \frac{v_1}{1 + v_1 - v_2} + \frac{y}{1 - v_1 + v_2}. \end{aligned} \quad (9)$$

## IV. RESULTS

In the past few years, the properties of quantum correlations in the LMG model, including the two-spin entanglement [43–46], entanglement entropy [47–49], multipartite entanglement [50–52], multipartite nonlocality [53], and quantum discord [54, 55], have been studied in depth. Besides, the fidelity susceptibility [56, 57], quantum Fisher information [58], as well as the Loschmidt echo and fidelity [59], have also been widely studied.

As quantum coherence is a fundamental property of quantum states and reflects the origin of quantum correlations [19–23], it is natural to speculate that the quantum coherence may also play a vital role in the understanding of quantum criticality in the high-dimensional systems. In particular, the two-spin entanglement in the LMG model decreases with the increase of the system size  $N$  for any  $h$  and vanishes in the large- $N$  limit [41], while the calculation of multipartite entanglement and nonlocality is intractable [50–53]. Quantum coherence and steered coherence, however, are not so sensitive to the variation of  $N$  and are analytically solvable. Thereby, it is expected that they may discover useful information of a many-body system. Motivated by these observations, we investigate in this section the ground-state coherence, ASC, and MSC in the LMG model, and carry out a scaling analysis of their dependence on the system size  $N$  in different phase regions.

### A. The thermodynamic limit

In the thermodynamic limit, a semiclassical approach gives the following mean-field wave function [60, 61]

$$|\psi(\theta, \phi)\rangle = \prod_{l=1}^N [\cos(\theta/2)e^{-i\phi/2} |\uparrow\rangle_l + \sin(\theta/2)e^{i\phi/2} |\downarrow\rangle_l], \quad (10)$$

with  $|\uparrow\rangle_l$  and  $|\downarrow\rangle_l$  being the eigenstates of  $\sigma_z^l$  with eigenvalues 1 and  $-1$ , respectively. Then one has

$$\langle \hat{H} \rangle = -\frac{(N-1)}{2} \sin^2 \theta (\cos^2 \phi + \gamma \sin^2 \phi) - hN \cos \theta, \quad (11)$$

and the ground state can be obtained by minimizing  $\langle \hat{H} \rangle$  over  $\theta$  and  $\phi$ . For such a model, a second-order QPT occurs at the critical point  $h = 1$ . In the region of  $h \geq 1$  (symmetric phase), the optimal angle  $\theta_0 = 0$ , all the spins are fully polarized in the direction of external magnetic field. In the region of  $0 \leq h < 1$  (broken phase),  $\theta_0 = \arccos h$ , the ground state will be twofold degenerate ( $\phi_0 = 0$  or  $\pi$ ) for  $\gamma \neq 1$  and infinitely degenerate ( $\phi_0$  can be arbitrary angle) for  $\gamma = 1$ .

We focus on  $\gamma < 1$  (the case of  $\gamma = 1$  is exactly solvable for any  $N$  and will be discussed in the next subsection). From Eq. (10) one can obtain that when  $h \geq 1$ ,  $v_1 = 1$ ,  $v_2 = y = u = 0$ . As a result,  $C_\alpha(\rho_{ij}^T) = C_\alpha^{\text{msc}}(\rho_{ij}^T) = 0$  and  $C_\alpha^{\text{asc}}(\rho_{ij}^T) = 2$  ( $\alpha = l_1$  or re), where we have denoted by  $\rho_{ij}^T$  the two-spin density operator in the thermodynamic limit. Thus when the system is in the symmetric phase, the three quantumness measures always remain constant, which is understandable as all the spins are

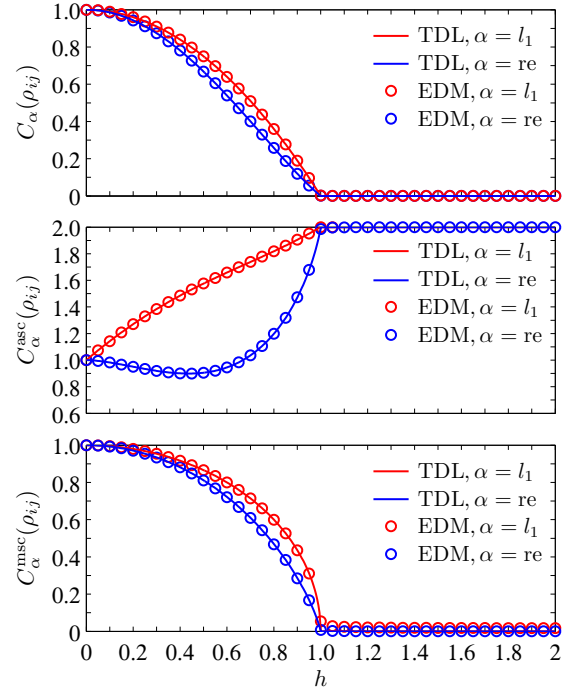


FIG. 1:  $C_\alpha(\rho_{ij})$ ,  $C_\alpha^{\text{asc}}(\rho_{ij})$ , and  $C_\alpha^{\text{msc}}(\rho_{ij})$  ( $\alpha = l_1$  or re) versus  $h$ , where the solid lines denote the thermodynamic limit (TDL) results and the circles denote the exact diagonalization method (EDM) results with  $\gamma = 0.5$  and  $N = 2^{12}$ .

fully polarized in the magnetic field direction and the system's ground state is  $|\uparrow\uparrow \dots \uparrow\rangle$ . Moreover, at first glance, it seems contradictory for the MSC to be zero and the ASC to be finite in the broken phase. But in fact there is no contradiction because they are defined in different bases, one is with respect to the eigenbasis of  $\rho_j$  which is state dependent, while the other one is with respect to the fixed mutually unbiased bases.

When  $0 \leq h < 1$ ,  $v_{1,2} = h_\pm^2/4$  and  $y = u = (1 - h^2)/4$ , where we have defined  $h_\pm = 1 \pm h$ . Then by making use of Eqs. (7), (8), and (9), one can obtain

$$\begin{aligned} C_{l_1}(\rho_{ij}^T) &= [C_{l_1}^{\text{msc}}(\rho_{ij}^T)]^2 = 1 - h^2, \quad C_{\text{re}}^{\text{msc}}(\rho_{ij}^T) = H_2\left(\frac{h_+}{2}\right), \\ C_{\text{re}}(\rho_{ij}^T) &= 1 + \frac{1+h^2}{2} \log_2(1+h^2) - \sum_{i=+,-} \frac{h_i^2 \log_2 h_i}{2}, \\ C_{l_1}^{\text{asc}}(\rho_{ij}^T) &= \frac{1 - h^2 + 3h + \sqrt{1+h^4-h^2}}{2}, \\ C_{\text{re}}^{\text{asc}}(\rho_{ij}^T) &= 2 - H_2\left(\frac{h_+}{2}\right) - H_2\left(\frac{1 + \sqrt{1+h^4-h^2}}{2}\right). \end{aligned} \quad (12)$$

In Fig. 1, we show  $h$  dependence of  $C_\alpha(\rho_{ij})$ ,  $C_\alpha^{\text{asc}}(\rho_{ij})$ , and  $C_\alpha^{\text{msc}}(\rho_{ij})$  for the thermodynamic limit result and the finite-size result of the exact diagonalization method. In the symmetric phase, as analyzed above, they always remain constant. In the broken phase, however, both  $C_\alpha(\rho_{ij})$  and  $C_\alpha^{\text{msc}}(\rho_{ij})$  ( $\alpha = l_1$  or re) decrease with the increase of  $h$ , whereas  $C_{l_1}^{\text{asc}}(\rho_{ij})$  increases with the increase of  $h$ , and  $C_{\text{re}}^{\text{asc}}(\rho_{ij})$  first decreases to a minimum of about 0.8991 and then turns to be increased to 2. The

coherence, ASC, and MSC can therefore be used as reliable detectors of QPT in this model. From Fig. 1 one can also see that the finite-size results with  $N = 2^{12}$  have good agreement with the mean-field results which are adaptive for the thermodynamic limit case.

### B. The isotropic case

For the isotropic LMG model (i.e.,  $\gamma = 1$ ), due to the global symmetries described by  $[\hat{H}, S^2] = 0$  and  $[\hat{H}, S_z] = 0$ , one has  $\langle \hat{H} \rangle = 2M^2/N - 2hM - N/2$ , with  $M = \langle S_z \rangle$ . By minimizing  $\langle \hat{H} \rangle$  over all  $M = -N/2, \dots, N/2$ , one can obtain immediately the ground state as  $|S, M_0\rangle$ , with

$$M_0 = \begin{cases} N/2 & \text{for } h \geq 1, \\ I(hN/2) & \text{for } 0 \leq h < 1, \end{cases} \quad (13)$$

where  $I(x)$  is the nearest integer (half-integer) from  $x$  for even (odd)  $N$ . When  $h \geq 1$ ,  $v_1 = 1$ ,  $v_2 = y = u = 0$ , so one still has  $C_\alpha(\rho_{ij}) = C_\alpha^{\text{msc}}(\rho_{ij}) = 0$  and  $C_\alpha^{\text{asc}}(\rho_{ij}) = 2$  ( $\alpha = l_1$  or re) in the symmetric phase region.

When  $0 \leq h < 1$ , by substituting  $M_0$  into Eq. (6) and using  $\langle S_x^2 \rangle = \langle S_y^2 \rangle$  for the ground state  $|S, M_0\rangle$ , one can obtain

$$\begin{aligned} C_\alpha(\rho_{ij}) &= C_{\text{re}}(\rho_{ij}) = \frac{N_+ N_-}{2N(N-1)}, C_{l_1}^{\text{msc}}(\rho_{ij}) = \frac{\sqrt{N_+ N_-}}{2N-2}, \\ C_{\text{re}}^{\text{msc}}(\rho_{ij}) &= H_2\left(\frac{N_+ - 1}{2N-2}\right) - H_2\left(\frac{1}{2} + \frac{\sqrt{N^2 + 12M_0^2}}{4N-4}\right), \\ C_{l_1}^{\text{asc}}(\rho_{ij}) &= x_0 + \frac{N_+ |1 - 2M_0| + N_-(N + 4M_0 + 1)}{2N(N-1)}, \\ C_{\text{re}}^{\text{asc}}(\rho_{ij}) &= 2 - 2H_2\left(\frac{1+x}{2}\right) + H_2\left(\frac{N_+}{2N}\right) \\ &\quad - \frac{N_+}{2N} H_2\left(\frac{N_-}{2N-2}\right) - \frac{N_-}{2N} H_2\left(\frac{N_+}{2N-2}\right), \end{aligned} \quad (14)$$

where we have denoted by  $N_\pm = N \pm 2M_0$  and  $x_0 = [N_+^2 N_-^2 + 16M_0^2(N-1)^2]^{1/2} / [2N(N-1)]$ . From Eq. (14), one can obtain that for large  $N$ , the coherence, ASC, and MSC show qualitatively the same  $h$  dependence to those shown in Fig. 1.

### C. Finite-size scaling

For the general LMG model with finite number of spins, the expectation values  $\langle S_z \rangle$  and  $\langle S_\alpha^2 \rangle$  ( $\alpha = x, y, z$ ) can be obtained approximately by means of the CUT method [62–64]. Different from the Holstein-Primakoff transformation method based on a first-order correction in the  $1/N$  expansion of the spin operators, the CUT method takes into account the higher-order corrections, thus enables the extraction of the finite-size scaling exponents of different observables [40, 41]. In the following, we first figure out the scaling formulae for the two-spin coherence, ASC, and MSC with the help of the CUT results of  $\langle S_z \rangle$  and  $\langle S_\alpha^2 \rangle$  ( $\alpha = x, y, z$ ) and then confirm them numerically

TABLE I: The coefficients  $a_\Phi$  ( $\Phi = z, xx, yy, zz$ ) obtained numerically with  $N = 2^{16}$  and different  $\gamma$ .

	$\gamma = 0$	$\gamma = 0.25$	$\gamma = 0.50$	$\gamma = 0.75$
$a_z$	-0.4599	-0.4182	-0.3659	-0.2913
$a_{xx}$	0.9188	0.8354	0.7307	0.5813
$a_{yy}$	1.1144	1.2257	1.4017	1.7621
$a_{zz}$	-0.9195	-0.8362	-0.7315	-0.5824

using the exact diagonalization method with the system size up to  $N = 2^{16}$ .

First, we consider scaling behaviors at the QPT point. The expectation values  $\langle S_z \rangle$  and  $\langle S_\alpha^2 \rangle$  ( $\alpha = x, y, z$ ) obtained via the CUT method can be found in Ref. [40]. For  $h = 1$  with very large but finite  $N$ , by considering the fact that there should be no singularity for any physical quantity in a finite system, one can obtain from Ref. [40] that

$$\begin{aligned} \frac{2\langle S_z \rangle}{N} &\sim 1 + \frac{1}{N} + \frac{a_z}{N^{2/3}}, \quad \frac{4\langle S_x^2 \rangle}{N^2} \sim \frac{a_{xx}}{N^{2/3}}, \\ \frac{4\langle S_y^2 \rangle}{N^2} &\sim \frac{a_{yy}}{N^{4/3}}, \quad \frac{4\langle S_z^2 \rangle}{N^2} \sim 1 + \frac{2}{N} + \frac{a_{zz}}{N^{2/3}}, \end{aligned} \quad (15)$$

where  $a_\Phi$  ( $\Phi = z, xx, yy, zz$ ) are the constants dependent on  $\gamma$ . Although their values cannot be determined with this scaling argument, we can obtain their approximate values by combining the above equation with the numerically obtained  $\langle S_z \rangle$  and  $\langle S_\alpha^2 \rangle$  ( $\alpha = x, y, z$ ) with very large  $N$ , see, e.g., the results listed in Table I, from which one can note that  $a_{zz} \approx 2a_z$ . Hence, by combining Eq. (15) with Eq. (6) and neglecting the exponentially small terms in  $1/N$ , one can obtain

$$\begin{aligned} y + u &\sim \frac{a_{xx}}{2N^{2/3}}, \quad y - u \sim -\frac{1}{2N}, \\ y + v_1 &\sim 1 + \frac{a_z}{2N^{2/3}}, \quad y - v_1 \sim -1 - \frac{a_z + a_{zz}}{2N^{2/3}}, \\ y + v_2 &\sim -\frac{a_z}{2N^{2/3}}, \quad y - v_2 \sim \frac{a_z - a_{zz}}{2N^{2/3}}, \\ v_1 + v_2 &\sim 1 + \frac{a_{zz}}{2N^{2/3}}, \quad v_1 - v_2 \sim 1 + \frac{a_z}{N^{2/3}}. \end{aligned} \quad (16)$$

When considering the  $l_1$  norm and relative entropy of coherence for the system at the critical point  $h = 1$ , as  $v_1 - v_2 \gg u$  for very large  $N$ , one can obtain from Eq. (7) that

$$C_{l_1}(\rho_{ij}) \sim \frac{a_{xx}}{N^{2/3}}, \quad C_{\text{re}}(\rho_{ij}) \sim -\frac{a_{zz}}{2N^{2/3}}, \quad (17)$$

thus the coherence of the two-spin state scales as

$$\log_2[C_\alpha(\rho_{ij})] \sim -\frac{2}{3} \log_2 N + \text{const}, \quad (18)$$

where  $\alpha = l_1$  or re, and the constant depends on  $\alpha$ ,  $\gamma$ , and  $h$  (likewise for those subsequent scaling formulae in other phase regions). Such a scaling behavior could be verified by diagonalizing the Hamiltonian  $\hat{H}$  numerically in the spaces spanned by  $\{|S, M_1\rangle\}$  ( $M_1 = -N/2, -N/2 + 2, \dots, N/2$ ) and  $\{|S, M_2\rangle\}$  ( $M_2 = -N/2 + 1, -N/2 + 3, \dots, N/2 - 1$ ) where the ground



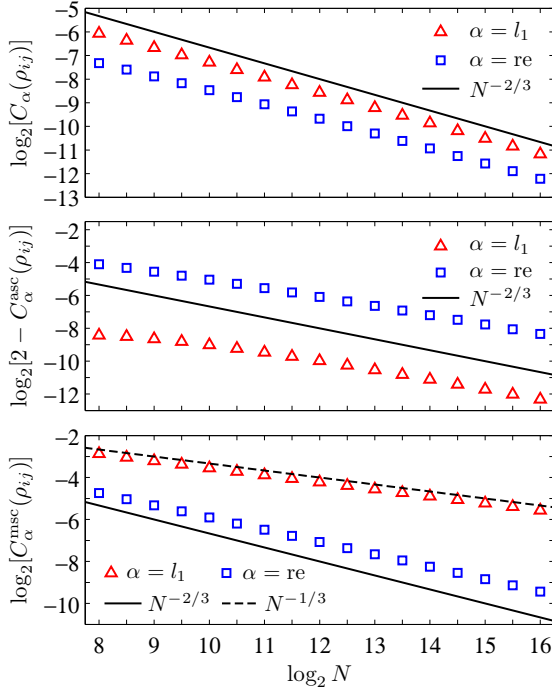


FIG. 2: Scaling behaviors of  $C_\alpha(\rho_{ij})$ ,  $C_\alpha^{\text{asc}}(\rho_{ij})$ , and  $C_\alpha^{\text{msc}}(\rho_{ij})$  ( $\alpha = l_1$  or re) at the QPT point  $h = 1$  with  $\gamma = 0.5$ . The slopes of the solid and dashed lines are  $-2/3$  and  $-1/3$ , respectively.

state lies in. For the system size up to  $N = 2^{16}$ , we display in the topmost panel of Fig. 2 the numerical results, from which one can note that  $\log_2[C_\alpha(\rho_{ij})]$  approaches the solid line with slope  $-2/3$  with an increase in  $\log_2 N$ .

For the ASC, by using the approximation  $(1+x)^{1/2} \simeq 1+x/2$  for very small  $x$ , one can obtain

$$\begin{aligned} x_{1,2} &\sim 1 + \frac{a_z}{N^{2/3}}, \quad \frac{y}{y+v_1} \sim -\frac{a_{zz}}{4N^{2/3}}, \\ \frac{y}{y+v_2} &\sim \frac{a_{zz}}{2a_z} + \frac{1}{a_z N^{1/3}}, \end{aligned} \quad (19)$$

and when the small  $x$  is positive, one also has  $H_2(x) \simeq x/\ln 2$ . These, together with Eqs. (8) and (16), yield

$$C_{l_1}^{\text{asc}}(\rho_{ij}) \sim 2 + \frac{4a_z + a_{xx}}{2N^{2/3}}, \quad C_{\text{re}}^{\text{asc}}(\rho_{ij}) \sim 2 + \frac{2a_z + a_{zz}}{4N^{2/3} \ln 2}, \quad (20)$$

where we have used the facts  $a_{xx} > 0$  and  $a_{zz} \simeq 2a_z < 0$  (Table I). So the ASC has the following finite-size scaling behavior:

$$\log_2[2 - C_\alpha^{\text{asc}}(\rho_{ij})] \sim -\frac{2}{3} \log_2 N + \text{const}, \quad (21)$$

where  $\alpha = l_1$  or re. This scaling formula was verified numerically by using the exact diagonalization method. As is shown in the middle panel of Fig. 2, the slope of  $\log_2[2 - C_\alpha^{\text{asc}}(\rho_{ij})]$  approaches  $-2/3$  gradually with an increase in  $N$ .

For the MSC, from Eqs. (9) and (16), one can obtain

$$r_{11} = \frac{a_{zz} + 2a_z}{4a_z} + \frac{a_{zz} + a_z}{4N^{2/3}}, \quad r_{12} = \frac{a_{xx}}{2\sqrt{-2a_z}N^{1/3}}, \quad (22)$$

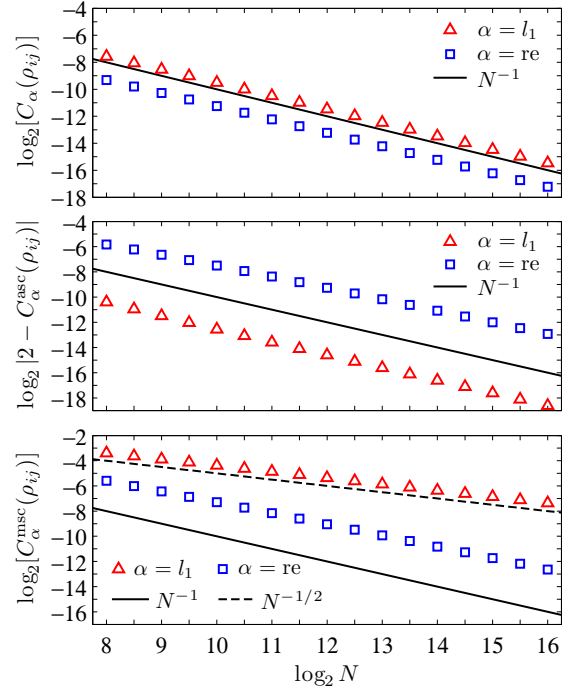


FIG. 3: Scaling behaviors of  $C_\alpha(\rho_{ij})$ ,  $C_\alpha^{\text{asc}}(\rho_{ij})$ , and  $C_\alpha^{\text{msc}}(\rho_{ij})$  ( $\alpha = l_1$  or re) in the symmetric phase with  $h = 1.1$  and  $\gamma = 0.5$ . The slopes of the solid and dashed lines are  $-1$  and  $-1/2$ , respectively.

then by substituting these into Eq. (8) and using the fact  $a_{zz} \simeq 2a_z$ , one can obtain

$$C_{l_1}^{\text{msc}}(\rho_{ij}) \sim \frac{a_{xx}}{\sqrt{-2a_z}N^{1/3}}, \quad C_{\text{re}}^{\text{msc}}(\rho_{ij}) \sim -\frac{a_{xx}^2}{4a_{zz}N^{2/3} \ln 2}, \quad (23)$$

which indicate that the two forms of MSC scale as

$$\begin{aligned} \log_2[C_{l_1}^{\text{msc}}(\rho_{ij})] &\sim -\frac{1}{3} \log_2 N + \text{const}, \\ \log_2[C_{\text{re}}^{\text{msc}}(\rho_{ij})] &\sim -\frac{2}{3} \log_2 N + \text{const}, \end{aligned} \quad (24)$$

thus different from coherence and ASC, the scaling exponents for the two forms of MSC are different. These scaling behaviors have also been verified numerically. As can be seen from the bottommost panel of Fig. 2, with the increase of the system size  $N$ , the slopes of  $\log_2[C_{l_1}^{\text{msc}}(\rho_{ij})]$  and  $\log_2[C_{\text{re}}^{\text{msc}}(\rho_{ij})]$  approach  $-1/3$  and  $-2/3$ , respectively.

Next, we consider scaling behaviors of the coherence, ASC, and MSC in the symmetric phase with  $h > 1$ . By denoting  $\Xi = (h-1)(h-\gamma)$ ,  $\gamma_\pm = 1 \pm \gamma$ , and neglecting those exponentially small terms in  $1/N$ , the CUT results of  $\langle S_z \rangle$  and  $\langle S_\alpha^2 \rangle$  ( $\alpha = x, y, z$ ) can be written as [40]

$$\begin{aligned} \frac{2\langle S_z \rangle}{N} &\sim 1 + \frac{b_z}{N}, \quad \frac{4\langle S_x^2 \rangle}{N^2} \sim \frac{b_{xx}}{N}, \\ \frac{4\langle S_y^2 \rangle}{N^2} &\sim \frac{b_{yy}}{N^{4/3}}, \quad \frac{4\langle S_z^2 \rangle}{N^2} \sim 1 + \frac{b_{zz}}{N}, \end{aligned} \quad (25)$$

with  $b_z = 1 + (\gamma_+ - 2h)/(2\Xi^{1/2})$ ,  $b_{xx} = (h-\gamma)/\Xi^{1/2}$ ,  $b_{yy} = 1/b_{xx}$ , and  $b_{zz} = 2b_z$ . Then, by combining Eq. (25) with Eqs. (6)–(9)

and after some algebra, one can obtain

$$\begin{aligned} C_{l_1}(\rho_{ij}) &\sim \frac{2b_0 - b_z}{N}, \quad C_{\text{re}}(\rho_{ij}) \sim -\frac{b_z}{N}, \\ C_{l_1}^{\text{asc}}(\rho_{ij}) &\sim 2 + \frac{2(b_0 + b_z)}{N}, \quad C_{\text{re}}^{\text{asc}}(\rho_{ij}) \sim 2 + \frac{b_z}{N \ln 2}, \\ C_{l_1}^{\text{msc}}(\rho_{ij}) &\sim \frac{2b_0 - b_z}{\sqrt{-2b_z N^{1/2}}}, \quad C_{\text{re}}^{\text{msc}}(\rho_{ij}) \sim -\frac{(2b_0 - b_z)^2}{8Nb_z \ln 2}, \end{aligned} \quad (26)$$

where we have defined  $b_0 = b_{xx} - b_{yy}$  for conciseness of Eq. (26). As  $b_{xx} > 1$ ,  $b_z < 0$ , and  $b_0 + b_z > 0$ , one can find that

$$\begin{aligned} \log_2[C_\alpha(\rho_{ij})] &\sim -\log_2 N + \text{const}, \\ \log_2[C_{l_1}^{\text{asc}}(\rho_{ij}) - 2] &\sim -\log_2 N + \text{const}, \\ \log_2[2 - C_{\text{re}}^{\text{asc}}(\rho_{ij})] &\sim -\log_2 N + \text{const}, \\ \log_2[C_{l_1}^{\text{msc}}(\rho_{ij})] &\sim -\frac{1}{2} \log_2 N + \text{const}, \\ \log_2[C_{\text{re}}^{\text{msc}}(\rho_{ij})] &\sim -\log_2 N + \text{const}, \end{aligned} \quad (27)$$

thus the scaling exponents for the two forms of coherence and ASC as well as for the relative entropy of MSC are  $-1$ , whereas it is  $-1/2$  for the  $l_1$  norm of MSC, see also Fig. 3. This is different from those scaling exponents at the QPT point. It indicates that with an increase in  $N$ ,  $C_\alpha(\rho_{ij})$  and  $C_\alpha^{\text{msc}}(\rho_{ij})$  in the symmetric phase decrease faster than those at the QPT point, while  $C_{\text{re}}^{\text{asc}}(\rho_{ij})$  increases faster than that at the QPT point. Besides,  $C_{l_1}^{\text{asc}}(\rho_{ij})$  decreases with the increase of  $N$  and approaches 2 in the thermodynamic limit, which is opposite to  $C_{l_1}^{\text{asc}}(\rho_{ij})$  at the QPT point.

Finally, by denoting  $\Lambda = 1 - h^2$  and neglecting those exponentially small terms in  $1/N$ , the CUT results of  $\langle S_z \rangle$  and  $\langle S_x^2 \rangle$  ( $\alpha = x, y, z$ ) in the broken phase can be obtained as [40]

$$\begin{aligned} \frac{2\langle S_z \rangle}{N} &\sim h + \frac{c_z}{N}, \quad \frac{4\langle S_x^2 \rangle}{N^2} \sim \Lambda + \frac{c_{xx}}{N}, \\ \frac{4\langle S_y^2 \rangle}{N^2} &\sim \frac{c_{yy}}{N}, \quad \frac{4\langle S_z^2 \rangle}{N^2} \sim h^2 + \frac{c_{zz}}{N}, \end{aligned} \quad (28)$$

with  $c_z = h(\gamma_-/\Lambda)^{1/2}$ ,  $c_{xx} = 2 + (\gamma h^2 + \gamma - 2)/(\Lambda \gamma_-)^{1/2}$ ,  $c_{yy} = h/c_z$ , and  $c_{zz} = 2hc_z + (\Lambda \gamma_-)^{1/2}$ . By combining Eq. (28) with Eqs. (6)–(9) and after some algebra, one can obtain

$$\begin{aligned} C_\alpha(\rho_{ij}) &\sim C_\alpha(\rho_{ij}^T) + \frac{a_\alpha}{N}, \quad C_\alpha^{\text{asc}}(\rho_{ij}) \sim C_\alpha^{\text{asc}}(\rho_{ij}^T) + \frac{b_\alpha}{N}, \\ C_\alpha^{\text{msc}}(\rho_{ij}) &\sim C_\alpha^{\text{msc}}(\rho_{ij}^T) + \frac{d_\alpha}{N}, \end{aligned} \quad (29)$$

where  $a_\alpha$ ,  $b_\alpha$ , and  $d_\alpha$  ( $\alpha = l_1$  or re) are complicated polynomials of  $\gamma$  and  $h$  given by

$$\begin{aligned} a_{l_1} &= \frac{c_0 - c_{zz}}{2}, \quad b_{l_1} = \frac{\kappa_2 + 3c_z + c_0}{2}, \quad d_{l_1} = \frac{c_0 - c_{zz}}{2\sqrt{\Lambda}}, \\ a_{\text{re}} &= \frac{\kappa_1}{4} \left[ \frac{1}{\ln 2} + \log_2 \left( \frac{1+h^2}{2} \right) \right] - \frac{c_{zz}}{2} \left( 1 + \frac{1}{\ln 2} \right) \\ &\quad + \frac{c_{zz} + 2c_z}{4} \log_2 \left( \frac{h_+^2}{4} \right) + \frac{c_{zz} - 2c_z}{4} \log_2 \left( \frac{h_-^2}{4} \right), \\ b_{\text{re}} &= \frac{\kappa_2}{2} \log_2 \left( \frac{\kappa_+}{\kappa_-} \right), \quad d_{\text{re}} = \kappa_3 \log_2 \left( \frac{h_-}{h_+} \right) + \frac{2\kappa_3 h + a_{l_1}}{2 \ln 2}, \end{aligned} \quad (30)$$

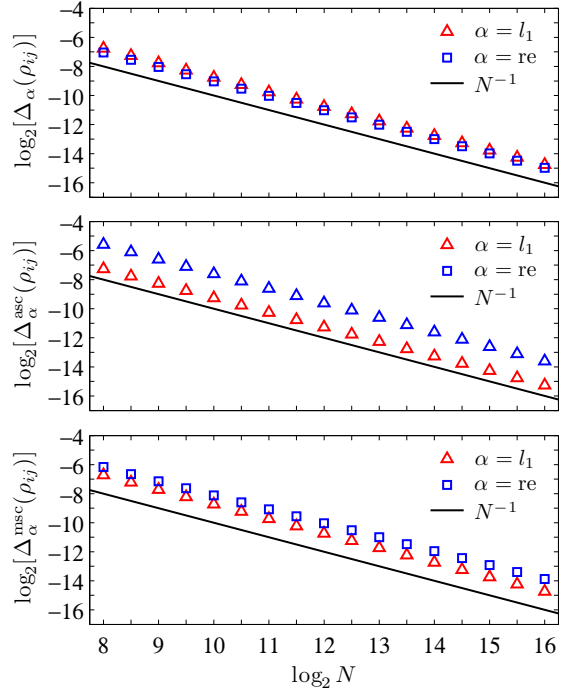


FIG. 4: Scaling behaviors of  $C_\alpha(\rho_{ij})$ ,  $C_\alpha^{\text{asc}}(\rho_{ij})$ , and  $C_\alpha^{\text{msc}}(\rho_{ij})$  ( $\alpha = l_1$  or re) in the broken phase with  $h = 0.9$  and  $\gamma = 0.5$ , where we have denoted by  $\Delta_\alpha(\rho_{ij}) = C_\alpha(\rho_{ij}^T) - C_\alpha(\rho_{ij})$ ,  $\Delta_\alpha^{\text{asc}}(\rho_{ij}) = C_\alpha^{\text{asc}}(\rho_{ij}) - C_\alpha^{\text{asc}}(\rho_{ij}^T)$ , and  $\Delta_\alpha^{\text{msc}}(\rho_{ij}) = C_\alpha^{\text{msc}}(\rho_{ij}^T) - C_\alpha^{\text{msc}}(\rho_{ij})$  in this plot, and the slopes of the solid lines are  $-1$ .

where  $c_0 = c_{xx} - c_{yy}$ ,  $\kappa_\pm = 1 \pm (\Lambda^2 + h^2)^{1/2}$ ,  $\kappa_1 = c_{zz} + (\Lambda c_0 + 4hc_z)/(1 + h^2)$ ,  $\kappa_2 = (hc_z + \Lambda a_1)/(\Lambda^2 + h^2)^{1/2}$ , and  $\kappa_3 = (2c_z - hc_{zz})/2\Lambda$ . Thereby the following scaling formulae hold:

$$\begin{aligned} \log_2[C_\alpha(\rho_{ij}^T) - C_\alpha(\rho_{ij})] &\sim -\log_2 N + \text{const}, \\ \log_2[C_\alpha^{\text{asc}}(\rho_{ij}) - C_\alpha^{\text{asc}}(\rho_{ij}^T)] &\sim -\log_2 N + \text{const}, \\ \log_2[C_\alpha^{\text{msc}}(\rho_{ij}^T) - C_\alpha^{\text{msc}}(\rho_{ij})] &\sim -\log_2 N + \text{const}, \end{aligned} \quad (31)$$

thus the scaling exponents are always  $-1$  in the broken phase, which are different from those at the QPT point. Such an observation has been confirmed by the numerical results shown in Fig. 4. It can be seen that the prediction of Eq. (31) works quite well. It also indicates that  $C_\alpha(\rho_{ij})$  and  $C_\alpha^{\text{msc}}(\rho_{ij})$  increase with the increase of the system size  $N$  and approach gradually to their thermodynamic limit values of  $C_\alpha(\rho_{ij}^T)$  and  $C_\alpha^{\text{msc}}(\rho_{ij}^T)$ , respectively, while  $C_\alpha^{\text{asc}}(\rho_{ij})$  decreases with the increase of the system size  $N$  and approaches gradually to  $C_\alpha^{\text{asc}}(\rho_{ij}^T)$ .

## V. SUMMARY AND DISCUSSION

To summarize, we have investigated coherence, ASC, and MSC of the LMG model which undergoes a second-order QPT with the increase of the transverse magnetic field. The motivation for considering such a problem is that coherence reflects the origin of quantumness, thus QPTs which correspond to dramatic changes of the ground state of a system,

might be tied to critical changes of coherence and the related quantities. Besides, the properties of coherence in the high-dimensional systems might be more complex and rich than that in the one-dimensional systems. Thereby, it is tempting to present a discussion of them.

We obtained analytical solutions of the two-spin coherence, ASC, and MSC for the thermodynamic limit and isotropic cases of the LMG model, and analyzed their properties by virtue of the exact diagonalization method for the general finite-size anisotropic case. The results showed that they show completely distinct behaviors in the symmetric phase and broken phase. These distinct behaviors can therefore be identified as reliable indicators of QPTs in the LMG model.

We have also obtained finite-size scaling exponents for the coherence, ASC, and MSC by using the CUT method and confirmed them numerically with the system size up to  $N = 2^{16}$ . It is found that the scaling behaviors are also phase dependent. Specifically, their behaviors are different in different phases, i.e., while the  $l_1$  norm of ASC shows opposite scaling behaviors at and out of the QPT point, the remaining quantities show opposite scaling behaviors in the broken and symmetric phases. These nontrivial behaviors can be attributed to the fact that they are generally nonlinear functions of the magnetization intensity  $\langle S_z \rangle$  and correlation function  $\langle S_\alpha^2 \rangle$  ( $\alpha = x, y, z$ ). So the same  $\langle S_z \rangle$  and  $\langle S_\alpha^2 \rangle$  at fixed magnetic field may yield different scaling behaviors of the coherence and steered coherence.

While the information uncovered by coherence and steered coherence may provide alternative perspective for understanding quantum criticality in the many-body systems, one may also concern the experimental verification of the connection between QPTs and coherence-based quantities established here. For this purpose, one may resort to the progresses on simulating the LMG model in trapped ions [34, 35], nitrogen-vacancy center ensembles [36], and superconducting qubits [37]. In particular, the dynamical phase transitions in the LMG model were experimentally observed in a quantum simulator with all-to-all connected superconducting qubits [37]. Hence, it is possible to expect a verification of these connections in future experiments with similar platforms.

## ACKNOWLEDGMENTS

This work was supported by the National Natural Science Foundation of China (Grant Nos. 11675129 and 11934018),

the Strategic Priority Research Program of Chinese Academy of Sciences (Grant No. XDB28000000), and Beijing Natural Science Foundation (Grant No. Z200009).

## Appendix A: Derivation of the MSC

As the reduced density operator  $\rho_j = \text{tr}_i \rho_{ij}$  is nondegenerate for  $h \neq 0$ , one only needs to take the maximization over the set of projective measurements  $M = (\mathbb{1} + \vec{m} \cdot \vec{\sigma})/2$  (see [28] for an explanation), where  $\vec{\sigma} = (\sigma_x, \sigma_y, \sigma_z)$  is a vector composed of the Pauli operators, and  $\vec{m}$  is a unit vector in  $\mathbb{R}^3$  with the polar and azimuth angles being denoted by  $\vartheta$  and  $\varphi$ , respectively.

For  $C_{l_1}^{\text{asc}}(\rho_{ij})$ , from Ref. [28] one can obtain

$$C_{l_1}^{\text{asc}}(\rho_{ij}) = \max_{\{\vartheta, \varphi\}} \frac{\sqrt{T_{11}^2 \cos^2 \varphi + T_{22}^2 \sin^2 \varphi} \sin \vartheta}{1 + (v_1 - v_2) \cos \vartheta}, \quad (\text{A1})$$

where  $T_{mn} = \text{tr}(\rho_{ij} \sigma_m \otimes \sigma_n)$ . It is direct to obtain that  $T_{11} = 2(y + u)$  and  $T_{22} = 2(y - u)$ , hence  $T_{11}^2 > T_{22}^2$ , and the optimal azimuth angle is given by  $\varphi_0 = 0$  or  $\pi$ . Besides, one can obtain directly the optimal polar angle as  $\vartheta_0 = \arccos(v_2 - v_1)$ . All these yield  $C_{l_1}^{\text{asc}}(\rho_{ij})$  in Eq. (8).

For  $C_{\text{re}}^{\text{asc}}(\rho_{ij})$ , we derive its expression as follows. First, the eigenbasis of  $\rho_j = \text{tr}_i \rho_{ij}$  is given by  $\{|0\rangle, |1\rangle\}$ . Within this basis, the postmeasurement state of spin  $j$  can be obtained as

$$\rho_{j|M} = \frac{1}{p_M} \begin{pmatrix} v_1 \cos^2 \frac{\vartheta}{2} + y \sin^2 \frac{\vartheta}{2} & \frac{\sin \vartheta}{2} (ue^{i\varphi} + ye^{-i\varphi}) \\ \frac{\sin \vartheta}{2} (ue^{-i\varphi} + ye^{i\varphi}) & v_2 \sin^2 \frac{\vartheta}{2} + y \cos^2 \frac{\vartheta}{2} \end{pmatrix}, \quad (\text{A2})$$

where  $p_M = y + v_2 + (v_1 - v_2) \cos^2(\vartheta/2)$ . Hence, according to its definition [28], the MSC is given by

$$C_{\text{re}}^{\text{asc}}(\rho_{ij}) = \max_{\{\vartheta, \varphi\}} \{S[(\rho_{j|M})_{\text{diag}}] - S(\rho_{j|M})\}, \quad (\text{A3})$$

then after some algebra, one can obtain that the optimal polar angle and azimuth angle related to  $M$  are still given by  $\vartheta_0 = \arccos(v_2 - v_1)$  and  $\varphi_0 = \{0, \pi\}$ , respectively. By inserting them into Eq. (A2), one can obtain the optimized  $\rho_{j|M}$  (we denote by  $r_{mn}$  its element lies in the  $m$ th row and  $n$ th column). Hence, we obtained  $C_{\text{re}}^{\text{asc}}(\rho_{ij})$  given in Eq. (8).

- 
- [1] S. Sachdev, *Quantum Phase Transitions* (Cambridge University Press, Cambridge, England, 2000).
  - [2] A. Osterloh, L. Amico, G. Falci, and R. Fazio, *Nature* **416**, 608 (2002).
  - [3] T. J. Osborne and M. A. Nielsen, *Phys. Rev. A* **66**, 032110 (2002).
  - [4] S. J. Gu, H. Q. Lin, and Y. Q. Li, *Phys. Rev. A* **68**, 042330 (2003).
  - [5] S. J. Gu, G. S. Tian, and H. Q. Lin, *Phys. Rev. A* **71**, 052322

(2005).

- [6] L. Amico, R. Fazio, A. Osterloh, and V. Vedral, *Rev. Mod. Phys.* **80**, 517 (2008).
- [7] K. Modi, A. Brodutch, H. Cable, T. Paterek, and V. Vedral, *Rev. Mod. Phys.* **84**, 1655 (2012).
- [8] A. Bera, T. Das, D. Sadhukhan, S. S. Roy, A. Sen(De), and U. Sen, *Rep. Prog. Phys.* **81**, 024001 (2018).
- [9] M. L. Hu, X. Hu, J. C. Wang, Y. Peng, Y. R. Zhang, and H. Fan, *Phys. Rep.* **762–764**, 1 (2018).

- [10] T. Baumgratz, M. Cramer, and M. B. Plenio, *Phys. Rev. Lett.* **113**, 140401 (2014).
- [11] A. Streltsov, G. Adesso, and M. B. Plenio, *Rev. Mod. Phys.* **89**, 041003 (2017).
- [12] J. J. Chen, J. Cui, Y. R. Zhang, and H. Fan, *Phys. Rev. A* **94**, 022112 (2016).
- [13] G. Karpat, B. Çakmak, and F. F. Fanchini, *Phys. Rev. B* **90**, 104431 (2014).
- [14] M. Qin, Z. Ren, and X. Zhang, *Phys. Rev. A* **98**, 012303 (2018).
- [15] S. G. Lei and P. Q. Tong, *Quantum Inf. Process.* **15**, 1811 (2016).
- [16] Y. C. Li and H. Q. Lin, *Sci. Rep.* **6**, 26365 (2016).
- [17] T. C. Yi, W. L. You, N. Wu, and A. M. Oleś, *Phys. Rev. B* **100**, 024423 (2019).
- [18] A. L. Malvezzi, G. Karpat, B. C. Çakmak, F. F. Fanchini, T. Debarba, and R. O. Vianna, *Phys. Rev. B* **93**, 184428 (2016).
- [19] A. Streltsov, U. Singh, H. S. Dhar, M. N. Bera, and G. Adesso, *Phys. Rev. Lett.* **115**, 020403 (2015).
- [20] X. Qi, T. Gao, and F. Yan, *J. Phys. A* **50**, 285301 (2017).
- [21] K. C. Tan, H. Kwon, C. Y. Park, and H. Jeong, *Phys. Rev. A* **94**, 022329 (2016).
- [22] Y. Yao, X. Xiao, L. Ge, and C. P. Sun, *Phys. Rev. A* **92**, 022112 (2015).
- [23] M. L. Hu and H. Fan, *Phys. Rev. A* **95**, 052106 (2017).
- [24] D. Mondal, T. Pramanik, and A. K. Pati, *Phys. Rev. A* **95**, 010301(R) (2017).
- [25] M. L. Hu and H. Fan, *Phys. Rev. A* **98**, 022312 (2018).
- [26] M. L. Hu, X. M. Wang, and H. Fan, *Phys. Rev. A* **98**, 032317 (2018).
- [27] X. Hu and H. Fan, *Sci. Rep.* **6**, 34380 (2016).
- [28] X. Hu, A. Milne, B. Zhang, and H. Fan, *Sci. Rep.* **6**, 19365 (2015).
- [29] M. L. Hu, Y. Y. Gao, and H. Fan, *Phys. Rev. A* **101**, 032305 (2020).
- [30] Y. X. Xie, *Phys. Status Solidi B* **258**, 2000322 (2021).
- [31] H. J. Lipkin, N. Meshkov, and A. J. Glick, *Nucl. Phys.* **62**, 188 (1965).
- [32] N. Meshkov, A. J. Glick, and H. J. Lipkin, *Nucl. Phys.* **62**, 199 (1965).
- [33] A. J. Glick, H. J. Lipkin, and N. Meshkov, *Nucl. Phys.* **62**, 211 (1965).
- [34] R. G. Unanyan and M. Fleischhauer, *Phys. Rev. Lett.* **90**, 133601 (2003).
- [35] A. Russomanno, F. Iemini, M. Dalmonte, and R. Fazio, *Phys. Rev. B* **95**, 214307 (2017).
- [36] Y. Zhou, S. L. Ma, B. Li, X. X. Li, F. L. Li, and P. B. Li, *Phys. Rev. A* **96**, 062333 (2017).
- [37] K. Xu, Z. H. Sun, W. Liu, Y. R. Zhang, H. Li, H. Dong, W. Ren, P. Zhang, F. Nori, D. Zheng, H. Fan, and H. Wang, *Sci. Adv.* **6**, eaba4935 (2020).
- [38] Y. C. Zhang, X. F. Zhou, X. Zhou, G. C. Guo, and Z. W. Zhou, *Phys. Rev. Lett.* **118**, 083604 (2017).
- [39] Y. C. Liu, Z. F. Xu, G. R. Jin, and L. You, *Phys. Rev. Lett.* **107**, 013601 (2011).
- [40] S. Dusuel and J. Vidal, *Phys. Rev. B* **71**, 224420 (2005).
- [41] S. Dusuel and J. Vidal, *Phys. Rev. Lett.* **93**, 237204 (2004).
- [42] X. Wang and K. Mølmer, *Eur. Phys. J. D* **18**, 385 (2002).
- [43] J. Vidal, G. Palacios, and R. Mosseri, *Phys. Rev. A* **69**, 022107 (2004).
- [44] J. Vidal, R. Mosseri, and J. Dukelsky, *Phys. Rev. A* **69**, 054101 (2004).
- [45] J. Vidal, *Phys. Rev. A* **73**, 062318 (2006).
- [46] J. Vidal, G. Palacios, and C. Aslangul, *Phys. Rev. A* **70**, 062304 (2004).
- [47] J. I. Latorre, R. Orus, E. Rico, and J. Vidal, *Phys. Rev. A* **71**, 064101 (2005).
- [48] V. Popkov and M. Salerno, *Phys. Rev. A* **71**, 012301 (2005).
- [49] T. Barthel, S. Dusuel, and J. Vidal, *Phys. Rev. Lett.* **97**, 220402 (2006).
- [50] H. T. Cui, *Phys. Rev. A* **77**, 052105 (2008).
- [51] A. C. Lourenço, S. Calegari, T. O. Maciel, and T. Debarba, *Phys. Rev. B* **101**, 054431 (2020).
- [52] R. Orús, S. Dusuel, and J. Vidal, *Phys. Rev. Lett.* **101**, 025701 (2008).
- [53] J. Bao, B. Guo, H. G. Cheng, M. Zhou, J. Fu, Y. C. Deng, and Z. Y. Sun, *Phys. Rev. A* **101**, 012110 (2020).
- [54] M. S. Sarandy, *Phys. Rev. A* **80**, 022108 (2009).
- [55] C. Wang, Y. Y. Zhang, and Q. H. Chen, *Phys. Rev. A* **85**, 052112 (2012).
- [56] H. M. Kwok, W. Q. Ning, S. J. Gu, and H. Q. Lin, *Phys. Rev. E* **78**, 032103 (2008).
- [57] J. Ma, L. Xu, H. N. Xiong, and X. Wang, *Phys. Rev. E* **78**, 051126 (2008).
- [58] J. Ma and X. Wang, *Phys. Rev. A* **80**, 012318 (2009).
- [59] Q. Wang, P. Wang, Y. Yang, and W. Wang, *Phys. Rev. A* **91**, 042102 (2015).
- [60] R. Botet, R. Jullien, and P. Pfeuty, *Phys. Rev. Lett.* **49**, 478 (1982).
- [61] R. Botet and R. Jullien, *Phys. Rev. B* **28**, 3955 (1983).
- [62] F. Wegner, *Ann. Phys. (Berlin)* **3**, 77 (1994).
- [63] S. D. Głazek and K. G. Wilson, *Phys. Rev. D* **48**, 5863 (1993).
- [64] S. D. Głazek and K. G. Wilson, *Phys. Rev. D* **49**, 4214 (1994).